ACTA IMEKO
ISSN: 2221-870X
June 2026, Volume 15, Number 2, 1 – 9

On the effectiveness of the Meteorological Optical Range for representing visibility as perceived by human drivers and by ADAS employing visible cameras

Davide Cassanelli[1], Stefano Cattini[1,2], Luigi Rovati[1,2]

[1] *Università degli studi di Modena e Reggio Emilia, Modena, Italy*
[2] *InterMech – MO.RE. Interdepartmental Centre for Applied Research and Services in Advanced Mechanics and Motor Engineering*

ABSTRACT
Adverse weather conditions continue to present a significant challenge for Advanced Driver Assistance Systems (ADAS). Quantification of visibility in fog is typically accomplished by measuring the Meteorological Optical Range (MOR). Despite the MOR's extensive recognition and utilisation across diverse domains, including aviation, navigation, and traffic management, there exists a potential discrepancy between the visibility estimated using the MOR, i.e. the optical path length in the atmosphere necessary to diminish the luminous flux of a collimated beam to 5 percent of its original value, and that actually perceived by drivers or camera-based ADAS systems operating within the visible range. Indeed, the anisotropy of the scattering generated by fog particles, in conjunction with the fact that, in the automotive sector, visibility is generally supported by the headlights and street lighting, can lead to phenomena not considered by the MOR. The present study proposes a measurement method and setup for investigating the degree to which visibility estimated exploiting the MOR represents the visibility perceived by drivers or camera-based ADAS systems. The experimental findings indicate that the lighting angle can substantially influence visibility. Thus, the study will propose a simplified analysis to identify the primary contributors to this discrepancy.

Section: RESEARCH PAPER

Keywords: fog; contrast; ADAS; illumination; imaging system

Citation: D. Cassanelli, S. Cattini, L. Rovati, On the effectiveness of the Meteorological Optical Range for representing visibility as perceived by human drivers and by ADAS employing visible cameras, Acta IMEKO, vol. 15 (2026) no. 2, pp. 1–9. DOI: 10.21014/actaimeko.v15i2.2266

Section Editor: Maik Rosenberger, Ilmenau University of Technology, Germany

Received: December 12, 2025; **In Final Form:** May 14, 2026; **Published:** June, 2026.

Funding: No funding specified.

Corresponding Author: Davide Cassanelli, e-mail: davide.cassanelli@unimore.it

1. INTRODUCTION

Reliable environmental perception under adverse weather conditions remains a major challenge for Advanced Driver Assistance Systems (ADASs) and autonomous vehicles. Fog represents a particularly complex scenario due to its strong scattering and absorption, which substantially degrade both driver visibility and the performance of ADAS sensors, such as cameras and LiDARs [1]–[7]. For human observers as well as for camera-based systems operating in the visible range (VIS), the capability to detect and distinguish targets within a foggy environment is strongly influenced by the characteristics and configuration of the light sources illuminating the scene, especially during nighttime.

Under favorable meteorological conditions, significant visibility limitations generally arise only at night. In these circumstances, as ambient illumination decreases and the sun is no longer the primary light source, the geometric arrangement, intensity, and distribution of artificial light sources—such as vehicle headlights and street lighting—play an increasingly critical role in determining visual performance. Conversely, under adverse weather conditions, including fog or heavy rainfall, visibility and contrast are markedly reduced even during daytime due to scattering and attenuation induced by the meteorological phenomena. Consequently, accurate knowledge and estimation of visibility in such conditions are essential to mitigate safety risks associated with missed detections or mis-detections of relevant targets.

Visibility is commonly characterized by the Meteorological Optical Range (MOR) [8], [9]. As will be better described in successive sections, the MOR can be computed by estimating the light attenuation due to an amount of fog along a defined optical path. Despite the MOR's extensive recognition and use across several domains, including aviation, navigation, and traffic management, there exists a potential discrepancy between the visibility estimated using the MOR and that actually perceived by drivers or camera-based ADAS systems operating within the

visible range (VIS). Indeed, a peculiarity of the automotive sector is that visibility is generally supported by light sources such as headlights on vehicles and street lighting. In consideration of the anisotropy of the scattering generated by fog particles and the concomitant dependence of this scattering on the incidence angle of the illuminants with respect to the observer, it is conceivable that the estimate provided by the MOR may not fully describe the visibility perceived by drivers or VIS-camera-based ADAS systems.

Several studies have investigated the use of onboard cameras and image contrast for visibility estimation. For instance, Graves et al. [10] proposed a solution based on predictive models which retrieve the image contrast in conditions of referenced visibility. Chen et al. [11] proposed a camera-based methodology for assessing visibility under varying ambient illumination conditions. Similarly, Hautière et al. [12] introduced a probabilistic model for visibility estimation derived from the distribution of image contrast. Yeo et al. [13] proposed a system based on the analysis of contrast of SWIR cameras. Moreover, [14] proposed a system based on a support vector machine, which used several image parameters, including the contrast, to predict the visibility.

In this study, a measurement method and setup are proposed for comparing visibility calculated in terms of beam attenuation, that is, in terms of MOR, and the visibility perceived by the driver or by a VIS-camera, which will be quantified by analyzing the contrast of the images acquired by means of a camera. Moreover, we propose an empirical interpretative model to analyze the experimental data from a theoretical point of view and compare the MOR with the contrast. This comparison will be made as the lighting angle, α, varies.

The manuscript is structured as follows. Section 2. describes the MOR definition and limitations, and the Weber contrast. Furthermore, it briefly introduces the theoretical framework of luminous flux transfer, which constitutes the basis for the analysis of image contrast, and recalls the theory describing the influence of fog on luminous flux. Section 3. details the proposed experimental methodology, based on the implemented measurement setup, and reports the outcomes of the experimental tests conducted with this setup. Section 4. introduces the empirical model developed to interpret variations in luminance and, consequently, in contrast, as a function of changes in the lighting angle α and fog density. In Section 5., the results obtained from the experimental measurements are compared with those predicted by the model and critically discussed. Finally, Section 6. summarizes the main findings and outlines future research directions stemming from the work presented.

2. THEORETICAL BACKGROUND

Figure 1 shows a schematic representation of a potential scenario on a city street. It is possible to observe that the illuminating angle α between the main vehicle (black car) and the light source can be widely different considering different sources: i) Main vehicle headlights $\alpha = 0°$: axial lighting, ii) Streetlights $0° < \alpha < 180°$ and iii) Other vehicle headlights $\alpha = 180°$: counter-axial lighting. These geometric variations can significantly influence the perceived contrast of objects seen by the driver or cameras on the main vehicle, and thus their detectability.

In foggy and highly scattering media, conventional visibility metrics may exhibit pronounced limitations. This section presents the theoretical framework, introducing the general principles of visibility assessment, the role of image contrast, and the fundamentals of luminous flux transfer in scattering media.

2.1. Meteorological Optical Range

The Meteorological Optical Range (MOR) is a widely employed parameter that serves to practically characterize the attenuation of light as it travels through fog. Recalling the definitions proposed by the World Meteorological Organization (WMO) [8], the ISO 28902-1:2012 standard [9] defines the MOR (for propagation through fog droplets) as: "the length of path in the atmosphere required to reduce the luminous flux in a collimated beam from an incandescent lamp, at a colour temperature of 2700 K, to 5 % of its original value". Then, the attenuation of luminance in a foggy environment can be approximately modeled using the Lambert-Beer law [8], [9]. According to the Lambert-–Beer law, and approximating the fog as a homogeneous medium, the illuminance of a collimated beam that propagates along the z-axis in a homogeneous medium is given by:

$$E(z) = E(0)\exp[-\sigma(\lambda)\cdot z]\,, \tag{1}$$

where σ is the extinction coefficient of the medium, λ is the wavelength radiation, and $E(0)$ is the illuminance at $z = 0$. Based on its definition, MOR relates to σ as [6], [9]:

$$MOR = \frac{3}{\sigma}. \tag{2}$$

However, the application of Lambert–Beer's law is strictly valid only when the propagation medium is purely absorbing. In the presence of significant scattering, as occurs for example in fog, its use constitutes a coarse approximation of the actual physical process. By definition, MOR neglects phenomena such as backscattering and veiling luminance. Nevertheless, these effects may lead to a reduction in the visibility perceived by a human driver.

2.2. Image contrast

As introduced in Section 1., the contrast can be employed to quantify the visibility of an observer. In the specific context of photography, numerous definitions of contrast have been proposed in the literature [15], [16]. In the present work, we adopt the Weber definition of contrast. Weber contrast quantifies the relative difference in luminance between an object and its background. From a physical and perceptual standpoint, it characterizes the perceived difference in luminance between a target and its surrounding background: the larger this relative difference, the more salient and easily detectable the target becomes. In accordance with (3), the Weber contrast is mathematically defined as:

$$C_{\mathrm{web}} = \frac{L_{\mathrm{T}} - L_{\mathrm{B}}}{L_{\mathrm{B}}}\,, \tag{3}$$

where L_{T} is the luminance of the target and L_{B} is the background luminance. This definition of contrast fits well with the analysis of an object's visibility in a foggy environment [14], [16]–[18]. Since contrast is determined by luminance, it inherently incorporates the influence of scattering within the medium. This relationship will be discussed in greater detail in the following section, where the basis of luminous flux transfer will be briefly recalled, and the impact of scattering on luminous flux will be introduced.

2.3. Luminous flux transfer in foggy environment

The analysis of the luminance L_{T} of a target, in an illuminated foggy environment, starts from the analysis of the luminous flux transfer from a point to another in space. The flux transfer analysis can be divided into two parts: i) the geometrical aspects of flux transfer and ii) the effects of the medium (fog) on light.

Let us consider a generic geometrical configuration consisting of three elements: a light source (LS), a target (TG), and an observer (O). Figure 2 shows the geometry discussed, comprehensive

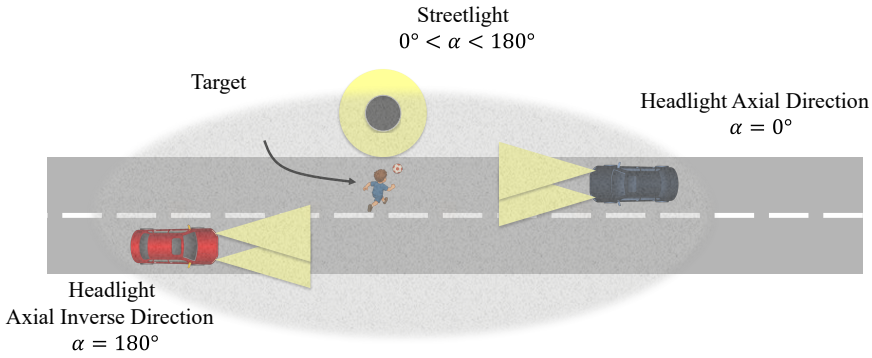

Figure 1. Schematic representation of a city street environment with different light sources illuminating a target.

of fog. The angles α and ψ are the illuminating angle with respect to the normal to the target and the normal to the LS respectively. The light source illuminates the target, which is located at a fixed distance R_{ST} from the source. Angles α and ψ are defined as the angles between the normals to the respective surfaces and the line segment connecting these surfaces. The light source emits radiation within a solid angular aperture Ω_{LS} and provides a constant total luminous flux Φ_{LS}. The target is assumed to behave as a Lambertian reflector. The visual axis of the observer is oriented in a manner that is both central and perpendicular to the surface of the target, with a distance R_{TO} measured from the target's surface. The fog introduces an attenuation coefficient σ.

Initially, we consider the geometry without the fog, thus in good visibility conditions. We can divide the geometry in two paths: light source-target (LS-TG) and target-observer (T-O). Let us start by analysing the flux transfer in the first path LS-TG. Each point on the target is subject to contributions of luminous flux from every infinitesimal element of the emitting source [19]. Even when the mathematical treatment is simplified by neglecting the absorption and scattering introduced by the fog, the luminous flux (Φ_{T}) that is incident on the target, originating from a light source, is given by the integral over both the source surface S_{LS} and the target surface S_{T}:

$$\Phi = \int_{S_{\mathrm{T}}} \int_{S_{\mathrm{LS}}} L_{\mathrm{LS}} \frac{\mathrm{d}s_{\mathrm{LS}} \cos(\psi)\, \mathrm{d}s_{\mathrm{T}} \cos(\alpha)}{R_{\mathrm{ST}}^2}\,, \tag{4}$$

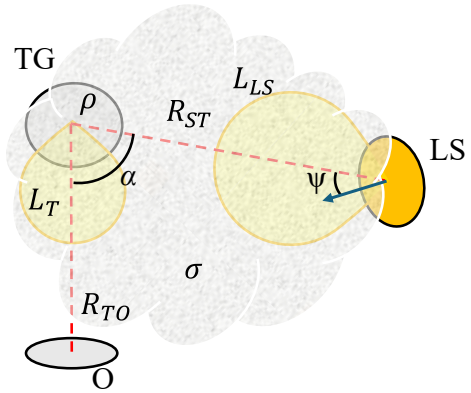

Figure 2. The schematic representation of the proposed geometric configuration is presented. The Light Source (LS) radiates the Target (TG) with a luminance L_{LS}. The angle ψ is defined between the normal vector $\vec{u}$ to the LS surface and the line of sight, while the angle α is defined between the normal vector $\vec{v}$ to the TG surface and the line of sight. The target is characterized by its reflectance, ρ. The spatial separation between the LS and TG is denoted as R_{ST}. The observer is positioned in alignment with the target, observing the reflected luminance from the target, noted as L_{T}. The distance between the target and the observer is defined as R_{TO}.

where $\mathrm{d}s_{\mathrm{LS}}$ and $\mathrm{d}s_{\mathrm{T}}$ are respectively the infinitesimal elements of the light source area and target area, and L_{LS} is the luminance of the light source. The parameter L_{LS} may, in general, depend on the angular emission characteristics of LS. This dependence substantially complicates the analytical treatment of the problem. To reduce this complexity, we employ the flat-top approximation for the light source, according to which L_{LS} is assumed to be spatially uniform over the entire emitting area of the source. The flux can be expressed in terms of flux per unit area or illuminance E by dividing Φ by the target area S_{T} removing the integration over the target area:

$$E = \int_{S_{\mathrm{LS}}} L_{\mathrm{LS}} \frac{\cos(\psi)\cos(\alpha)\, \mathrm{d}s_{\mathrm{LS}}}{R_{\mathrm{ST}}^2}\,, \tag{5}$$

Equation (5) is, in most cases, analytically intractable without comprehensive knowledge of the source's radiance distribution and the exact geometry of the surfaces involved; consequently, such simplifying assumptions are conventionally adopted.

Assume that the source can be approximated as a point emitter positioned at a distance R_{ST} from the target. This approximation is justified when the dimensions of the source are less than 10 % of R_{ST}, and the emission is spatially uniform within the illumination cone (flat-top approximation) [19]. Under this point-source approximation, the illuminance E on the target reduces to the inverse-square law form:

$$E = \frac{L_{\mathrm{LS}}\, S_{\mathrm{LS}} \cos(\psi)\cos(\alpha)}{R_{\mathrm{ST}}^2}\,. \tag{6}$$

From the definition of luminous flux and luminance, L_{LS} can be written as:

$$L_{\mathrm{LS}} = \frac{\Phi_{\mathrm{LS}}}{\Omega_{\mathrm{LS}}\, S_{\mathrm{LS}}}\,. \tag{7}$$

By replacing (7) in (6), it is possible to express E_{T} as:

$$E = \frac{\Phi_{\mathrm{LS}}}{\Omega_{\mathrm{LS}}} \frac{\cos(\alpha)\cos(\psi)}{R_{\mathrm{ST}}^2}\,. \tag{8}$$

For a Lambertian target of diffuse reflectance ρ, the reflected luminance L_0 is related to the local illuminance E by:

$$L(\alpha,\psi) = \frac{\rho}{\pi} E\,. \tag{9}$$

Substituting (8) gives:

$$L_0(\alpha,\psi) = \rho\, \frac{\Phi_{\mathrm{LS}}}{\Omega_{\mathrm{LS}}\, \pi} \frac{\cos(\alpha)\cos(\psi)}{R_{\mathrm{ST}}^2}\,. \tag{10}$$

Equation (10) gives the target luminance as observed by the observer, in good visibility conditions.

In conditions of reduced visibility due to fog, the propagation of light between the source, the target, and the observer is significantly influenced by both absorption and scattering processes. The accurate quantification of light intensity reaching both the target and the observer requires solving the radiative transfer equation, a task that is inherently intricate and frequently defies analytic solutions. This complexity arises because light propagation in scattering media, such as fog, involves multiple scattering interactions. Considering the proposed geometry, the attenuated component of the luminance generated by the light source that reaches the observer after being reflected by the target is given by (11), considering L_0 the target luminance in the absence of fog and a medium with an attenuation coefficient σ.

$$L_{\mathrm{obs}} = L_0 \exp[-\sigma\,(R_{\mathrm{ST}} + R_{\mathrm{TO}})]\,. \tag{11}$$

As previously introduced, fog is a scattering media, thus it introduces other effects which can affect the observed luminance. Fog also contributes to the observed luminance with an additive effect called veiling [17], [18], [20]–[22]. Briefly recalling the effects of these phenomena on luminance, back-scattering occurs when light strikes suspended particles and is reflected directly back towards the observer, creating a blinding glare that obscures objects behind the fog. Veiling arises from the scattering of radiation along the line of sight, introducing an additional "veil" luminance component between the observer and the observed target. Both phenomena are governed by the physical properties of fog droplets (e.g., number density, particle size distribution) and contribute additively to the resulting luminance [17], [20]. Consequently, the total luminance observed in foggy conditions can be expressed as:

$$L_{\mathrm{obs-tot}} = L_0 \exp[-\sigma\,(R_{\mathrm{ST}} + R_{\mathrm{TO}})] + L_{\mathrm{fog}}\,, \tag{12}$$

where L_{fog}, fog luminance, represents the additive terms introduced by back-scattering and veiling. The analytical derivation of this term within a rigorous theoretical framework is complex and requires the solution of the radiative transfer equation, as well as a detailed characterization of the physical properties of the propagation medium. Consequently, it can be obtained either by means of Monte Carlo simulations or through empirical estimation. In this study, we introduce an experimental procedure for the direct evaluation of the fog luminance L_{fog}.

Therefore, equation (12) allows to describe the luminance of a target as a function of the geometry of the target and the light source in a foggy environment. This luminance can then be used to calculate the Weber contrast of a target by substituting (12) into (3) and evaluating the visibility for an observer. It can be noted that a visibility assessment based on contrast therefore takes into account the additional effects of back-scattering and veiling, unlike the MOR definition.

3. EXPERIMENTAL METHOD

The analysis of contrast as a function of the illumination angle in a foggy environment is conducted through an experimental procedure in which the fog is confined within a Fog Chamber (FC). This methodology is based on the light attenuation, thus the MOR, estimation through the Lambert–Beer law [21], [23]. Under this approximation, an optical path characterized by a given average fog concentration can be approximated by an equivalent path composed of a fog-free section and a section immersed in fog (corresponding to the FC length), in which the fog concentration is chosen such that it matches the effective average fog concentration of the original path. In this section, we will describe the experimental setup and the measurement procedure used to evaluate contrast of an image in a foggy environment and its relative perceived visibility.

3.1. Experimental setup

The experimental setup follows the geometry presented in Figure 2. The fog generation and confinement system is similar to that described in [5], [6] and consists of a chamber in which the fog is contained throughout the testing procedures. Figure 3 schematically illustrates the measurement setup.

The observer O is a CMOS camera (BFS-U3-50S5M-C, Flir, Oregon, US) with a 16 mm objective (M23F16V, Tamron, Saitama, Japan). The camera is placed on one side of the FC, aligned with the target TG. The target TG is a white circular crown (minimum radius $r_1 = 10$ cm and maximum radius $r_2 = 15$ cm) painted with acrylic white paint attached to a sheet of black paper. The choice of this target was made since it is symmetrical in all directions, being formed by concentric circles, and, more importantly, it allows contrast to be calculated taking only the object into account. Considering Weber's definition, our real target will be the black circle inside the crown, while the background will be the white crown itself. The distance between the camera and the target is $R_{\mathrm{TO}} = 1$ m. The light source is an LED lamp (MR16 50 by Osram, Germany, with an illumination conical beam of $\Omega_{\mathrm{LS}} = 36°$), which is attached to the FC with a rotating aluminium arm, allowing the variation of the illumination angle α to the camera optical axis. The rotating arm is attached to a rotating stage OCT-XYR1/M (Thorlabs, Inc., New Jersey, US). The illumination angle α is varied from 0° to 85° in discrete steps of $\Delta\alpha = 5°$. The lamp is oriented toward the target, with its axis of rotation coincident with the center of the target. Consequently, the distance between the lamp and the target remains constant throughout the rotation. The distance between the light source and the target is $R_{\mathrm{ST}} = 1.10$ m. A Laser Diode - Photodiode

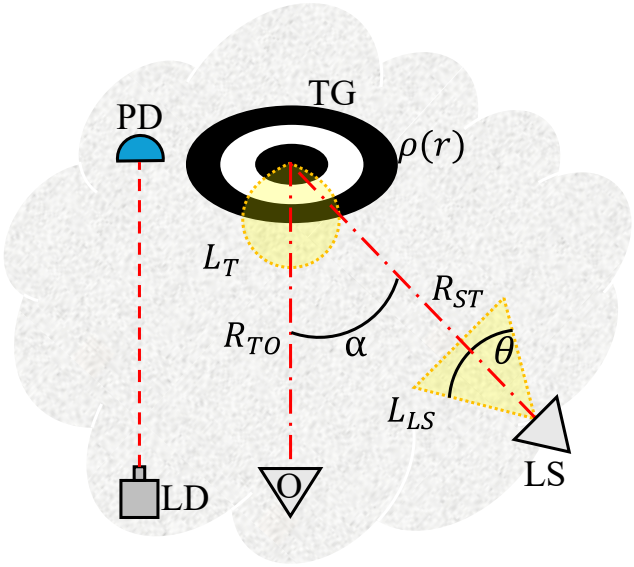

Figure 3. Schematic representation of the measurement setup. The LS, a LED lamp, has a conical beam with emission angle θ. The LS is aligned with the target to have $\phi = 0°$, while its direction forms an angle α with the normal to the target. The angle can be varied through a rotating stage. The fixed distance between the LS and the target is R_{ST}. The target has a total radius of r_0 and consists of concentric black and white rings and reflectance which depends on the radius. The observer, a CMOS camera, is aligned with the target at a fixed distance R_{TO}. The observer sees the luminance $L_{\mathrm{obs-tot}}$ generated by the light source that reaches the observer after being reflected by the target emitted by the target or the fog. The LD-PD system is used for evaluate the MOR during the measurements.

couple (LD-PD) is placed on the same plane as the camera and lamp to monitor the light attenuation due to fog. The PD current I is used to evaluate the extinction coefficient σ at different fog levels according to equations (1) and (2). This LD-PD system is used to obtain a reference value for attenuation and, thus, for MOR, since such a system is unaffected by the illumination angle. The whole system is controlled by a host PC running a MATLAB script, responsible for the acquisition of camera images, LD-PD signal acquisition, fog generation, and illumination control.

3.2. Measurement procedure

The experimental analysis is based on a measurement procedure involving five steps. This procedure was repeated for $j = 1..M$ lighting angular positions ranging from $\alpha = 0°$ to $\alpha = 85°$. Prior to initiating the measurements, a warm-up time was observed to allow for the instruments to reach an equilibrium temperature.

1) Complete clearing of the FC from fog.
2) Baseline acquisition of PD current $I_{\mathrm{ref}}(j)$ and reference target image $F_{\mathrm{ref}}(j)$ in the best visibility condition (i.e., in the absence of fog).
3) Generation of fog and its injection into the FC.
4) Suspension of fog generation and acquisition of $i = 1..N$ samples of PD current $I(j,i)$ and camera images $F(j,i)$ at a sampling frequency f.
5) Change of the angle of incidence α.

After the FC was filled, fog generation was stopped and the acquisition of the target images, $F(j,i)$, and the light attenuation data, $I(j,i)$, were initiated. During this phase, the fog density gradually decreased as it naturally dissipated through a small vent. Following the acquisition phase, the data obtained were analyzed. According to (3), the Weber contrast for each acquisition $C(j,i)$ can be determined by extracting the luminance values of the target and the background (in this case, the black circle and the white crown, respectively). Since the camera gray-level intensity J is proportional to the luminance that reaches the photodetector, scaled by the intrinsic parameters of the camera, it is possible to directly use the pixel intensities corresponding to the black circle and to the white crown to compute the Weber contrast. The relationship between luminance L and pixel intensity can be expressed as:

$$J = G \cdot L\,, \tag{13}$$

where G is a conversion term which depends on the camera setting (sensor type, gain, exposure time, optics). Therefore, for each acquired image, the average gray level intensity of the black region, $\bar{J}_{\mathrm{B}}(j,i)$, and the average gray level intensity of the white region, $\bar{J}_{\mathrm{W}}(j,i)$, were extracted and used for the target luminance, L_T, and the background luminance, L_{BG}, respectively, in (3). The experimentally derived contrast $C_{\mathrm{e}}(j,i)$ was then calculated for each acquisition and for each angle of illumination. The collected data were processed by first computing the $MOR(j,i)$, obtained from the light attenuation measurements acquired with the LD–PD system. Subsequently, the contrast $C_{\mathrm{e}}(j,i)$ of each captured target image was evaluated. Therefore, the Weber contrast of the i-th captured image at the j-th illumination angle is given by:

$$C_{\mathrm{e}}(i,j) = \frac{\bar{J}_{\mathrm{B}} - \bar{J}_{\mathrm{W}}}{\bar{J}_{\mathrm{W}}}\,, \tag{14}$$

As reported in Section 2.1. the MOR is given by Equation (2). Hence, the MOR of the i-th acquisition at the j-th illumination angle is related to $\sigma(j,i)$, that, from (1), can be computed as:

$$\sigma(j,i) = \frac{1}{R_{\mathrm{TO}}} \ln\left[\frac{E(j,i,0)}{E(j,i,R_{\mathrm{TO}})}\right]\,, \tag{15}$$

where $E(j,i,0)$ and $E(j,i,R_{\mathrm{TO}})$ represent the illuminance entering and leaving the FC during the i-th acquisition with j-th angle. Based on the experimentally verified assumption of a stable LD source and the conservation of illuminance within a fog-free FC, the input illuminance $E(0°,i)$ is derived from the output illuminance measured during the baseline. Since the PD current $I(j,i)$ is proportional to the outgoing illuminance $E(j,i,R_{\mathrm{TO}})$, the attenuation coefficient for the i-th acquisition at the j-th angle is derived as:

$$\sigma(j,i) = \frac{1}{R_{\mathrm{TO}}} \ln\left[\frac{I_{\mathrm{ref}}(j)}{I(j,i)}\right] \tag{16}$$

Thus, the MOR of the i-th acquisition at the j-th angle is:

$$MOR(j,i) = R_{\mathrm{TO}} \cdot 3 \cdot \left\{\ln\left[\frac{I_{\mathrm{ref}}(j)}{I(j,i)}\right]\right\}^{-1}\,. \tag{17}$$

3.3. Results

This section presents the results of the experimental analysis of the experimentally observed contrast C_e. By way of example, Figure 4 shows the acquired images of the target with illumination angles α respectively equal to 0°, 45°, and 85°, in both clear and heavy fog conditions ($MOR \approx 2.4\,\mathrm{m}$). Looking at the images in foggy conditions, it is possible to see that when the angle is $\alpha = 0°$, the fog luminance component is pronounced, applying a luminous glow over the image. When the angle is $\alpha = 45°$, this component is less present, and the image appears as if it were only attenuated. Finally, when the angle is $\alpha = 85°$, the veil luminance effect is barely visible; however, the low illuminance makes the image quite dark. The results of Weber contrast and perceived visibility analysis are shown in Figure 5. These results will be discussed in Section 5..

4. SIMPLIFIED GEOMETRICAL MODEL

The experimental analysis enables the derivation of results for specific configurations associated with the proposed setup. However, the formulation of a simplified model allows for a better interpretation of the experimental results reported in Section 3.3. and highlights the contributions that lead to different behaviors of MOR and contrast. A comprehensive model that fully accounts for the visibility behavior of a target immersed in fog and illuminated by a given light source is a highly complex undertaking, as it requires solving the complete radiative transfer equation. Therefore, we introduce a simplified model grounded in empirical results obtained through the measurement procedure described in Section 3.2.. This model is constructed based on the geometry of the general case illustrated in Figure 2 and on the experimental configuration depicted in Figure 3. The light source (LS) is modeled as a lamp emitting a conical luminous beam characterized by an emission angle θ, which corresponds to a solid angle given by $\Omega_{\mathrm{LS}} = 2\,\pi\left(1 - \cos\left(\frac{\theta}{2}\right)\right)$. The LS is oriented such that its optical axis passes through the center of the target; hence, the angle between the normal vector to the illuminated surface and the line segment connecting the LS to the target (LS–TG) is $\psi = 0°$. The observer O is positioned along the surface normal of the target, forming an angle α with the propagation direction of the LS. Under these conditions, equation (10) simplifies to:

$$L_{\mathrm{T}}(\alpha) = \rho \frac{\Phi_{\mathrm{T}}}{\Omega_{\mathrm{LS}} + \pi} \frac{\cos(\alpha)}{R_{\mathrm{ST}}^2} = L_{\mathrm{T}}(0) \cdot \cos(\alpha)\,, \tag{18}$$

where R_{ST} is the fixed distance between the LS and the target. The target, recalling the experimental target, is a black and white

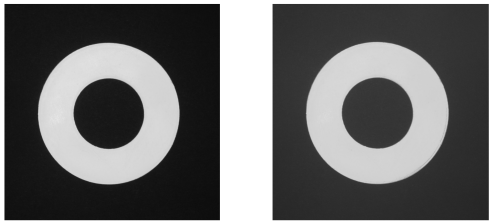

(a) $\alpha = 0°$ $MOR > 1000$ m (b) $\alpha = 0°$ $MOR = 2.5$ m

(c) $\alpha = 45°$ $MOR > 1000$ m (d) $\alpha = 45°$ $MOR = 2.4$ m

(e) $\alpha = 85°$ $MOR > 1000$ m (f) $\alpha = 85°$ $MOR = 2.4$ m

Figure 4. Example of image acquisition in clear and foggy conditions. Figures (a) and (b) show the target with $MOR > 1000$ m and $MOR = 2.5$ m at $\alpha = 0°$. Figures (c) and (d) show the target in good visibility and $MOR = 2.4$ m at $\alpha = 45°$. Figures (e) and (f) show the target in good visibility and $MOR = 2.4$ m at $\alpha = 85°$.

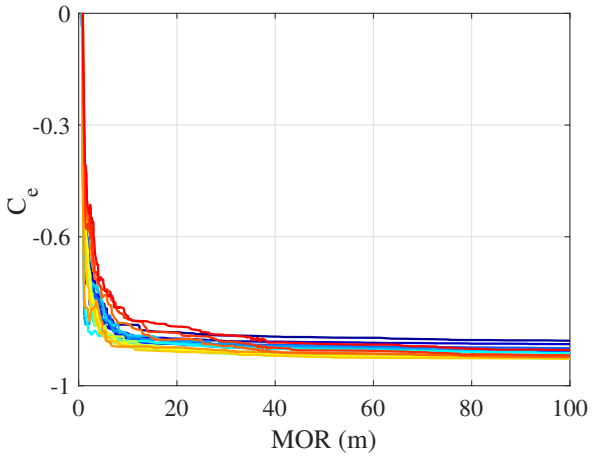

Figure 5. Results of the Weber contrast experimental analysis at different illuminating angles in foggy conditions. Behavior of experimental Weber contrast C_e as a function of MOR. Legend: — 0°, — 5°, — 10°, — 15°, — 20°, — 25°, — 30°, — 35°, — 40°, — 45°, — 50°, — 55°, — 60°, — 65°, — 70° c, — 75°, — 80°, — 85°.

circle, like the one in Figure 6, with a reflectance that varies along

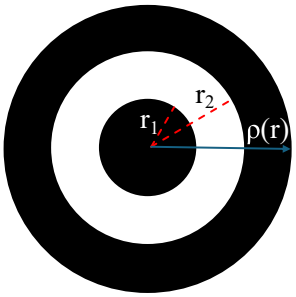

Figure 6. Target used for the model. The reflectance depends on the radius following (19).

the radius $\rho(r)$ as:

$$\rho(r) = \begin{cases} \rho_1 & : r \leq r_1 \\ \rho_2 & : r_1 \leq r \leq r_2 \\ \rho_1 & : r \geq r_2 \,. \end{cases} \tag{19}$$

As delineated in Section 2., the source was approximated as exhibiting a uniform flat-top radiance distribution, while being modeled as a point-like emitter. The target was assumed to be perfectly planar and Lambertian. Within the theoretical framework introduced in Section 2.3., this modeling permits the computation of the illuminance of the LS on the target, and, subsequently, the determination of the corresponding reflected luminance. On this basis, the Weber contrast of the simulated scene can be evaluated. For the purposes of the experimental measurements, the white crown is treated as the background, whereas the black circle is considered the actual target in the Weber contrast calculation.

4.1. Empirical fog luminance

Recalling the expression for luminance observed in fog, (12), the fog luminance L_{fog}, representing the additive terms of back-scattering and veiling, cannot be obtained in closed form from theory alone. Therefore, this quantity must be estimated either through numerical simulations or by means of experimental measurements. In the present study, we opted to determine the fog luminance empirically, using the results obtained from the experimental analysis described in the preceding section. Indeed, from (12), given the luminance L_0 under good visibility conditions ($L_{\text{fog}} = 0$) and the luminance $L_{\text{obs-tot}}$ at a specific fog level, the fog luminance for a given geometric configuration can be retrieved as:

$$L_{\text{fog}} = L_{\text{obs-tot}} - L_0 \cdot \exp(-\sigma \cdot R_{\text{tot}}) \,, \tag{20}$$

where σ is the attenuation coefficient of the medium and $R_{\text{tot}} = R_{\text{ST}} + R_{\text{TO}}$ is the total optical path traveled by the light from the source to the observer. From the results presented in Section 3.3., it is possible to estimate the fog luminance, expressed in terms of the image gray-level intensity measured by the camera, J_{fog}, which is proportional to the physical fog luminance L_{fog}. Since our objective is to characterize the visibility as perceived by the camera, rather than the absolute contrast of the target, all luminance measurements are converted into corresponding camera gray-level intensity. This allows us to compute a contrast metric directly comparable to the experimental image data.

4.2. Contrast calculation

The aim of this work is to show how contrast takes into account the additive effects of back-scattering and veiling luminance. As previously described, contrast is based on the definition of luminance, therefore, since luminance includes fog luminance L_{fog}, it is legitimate to argue that contrast itself takes this phenomenon

into account.

To explain how veil luminance affects contrast, we can start by rewriting Weber's definition of contrast to highlight the illumination angle. Hence, by replacing (10) in (3), and defining the luminance at $\alpha = 0°$ as $L_0(0°)$, the Weber contrast can be rewritten as in (21). We only consider angle α, however the same reasoning can be done for ψ.

$$C_{\text{web}-0} = \frac{[L_{\text{t}}(0°) - L_{\text{bg}}(0°)]\ \cos(\alpha)}{L_{\text{bg}}(0°)\ \cos(\alpha)} = \frac{L_{\text{t}}(0°) - L_{\text{bg}}(0°)}{L_{\text{bg}}(0°)}\,. \tag{21}$$

As evident from (21), the Weber contrast is independent of the illumination angle α, thus it must be constant when moving the LS. Nevertheless, if we consider the fog effect, and we substitute (12) into (3), the contrast assumes this form:

$$\begin{aligned} C_{\text{web}} &= \frac{L_{\text{t}}\,T + L_{\text{fog}} - L_{\text{B}}\,T - L_{\text{fog}}}{L_{\text{B}}\,T + L_{\text{fog}}}\,, \\ T &= \exp(-\sigma\,(R_{\text{ST}} + R_{\text{TO}}))\,, \end{aligned} \tag{22}$$

that can be reduced to:

$$C = \frac{[L_t(0°) - L_{bg}(0°)]T\cos(\alpha)}{L_{bg}(0°)T\cos(\alpha) + L_{fog}}\,. \tag{23}$$

Equation (23) shows that Weber's contrast depends on the amount of fog, decreasing in particular as the veiling/backscattering effect induced by the fog increases. In particular, for small values of T (low visibility), the contrast is reduced to (24), showing a hyperbolic decay as L_{fog} increases. Therefore, the contrast for low visibility values depends on L_{fog}, which by definition depends on how the fog bank is illuminated and therefore on the illumination angle α.

$$C \approx \frac{1}{L_{\text{fog}}}\,. \tag{24}$$

As it is possible to observe, the Weber contrast is strongly affected by L_{fog}, thus its analysis takes into account the scattering phenomena which MOR ignores. Knowing the expression of Weber contrast in foggy environment, it is possible to apply it to our geometrical model to evaluate the contrast behavior in fog. The model requires as input the following parameters:

- The total luminous flux of the light source Φ.
- The emission angle θ of the light source.
- The distances between the light-emitting source and the designated target R_{ST}, as well as the separation between the target and the observer R_{TO}.
- The MOR values for which we want to evaluate the contrast.
- The empirically derived J_{fog} for the MOR and for each illuminating angle α.
- The empirical conversion parameter G.

First, the input parameters were used to retrieve the illuminance E on the target and the relative reflected luminance L_0 in absence of fog for $\alpha = 0°$ as defined in (10) for both the black and white region of the target. Then the transmittance $T = \exp(-\sigma \cdot (R_{\text{ST}} + R_{\text{TO}}))$ was computed retrieving the attenuation coefficient σ from equation (2) for each MOR values. Subsequently, the luminance of the entire target in the presence of fog, considering only the attenuation effect L_{obs}, was calculated following (11) and mapped in terms of pixel intensity through the factor G. At this point, we can apply (23) to compute, for each angle and for each MOR value, the contrast $C_{\text{m}}(\alpha, MOR)$.

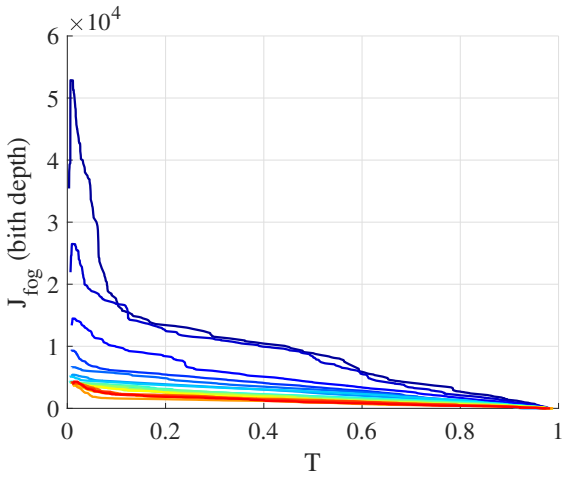

Figure 7. Empirically derived fog luminance in camera gray level intensity (from 0 to $2^{16} - 1$), with respect to the transmissivity T. Legend: 0°, 5°, 10°, 15°, 20°, 25°, 30°, 35°, 40°, 45°, 50°, 55°, 60°, 65°, 70°, 75°, 80°, 85°.

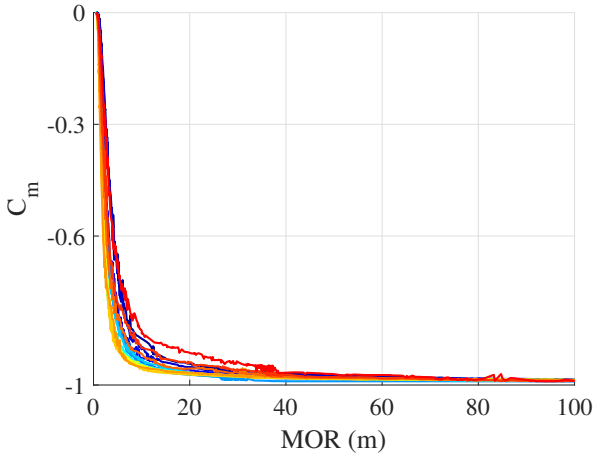

Figure 8. Results of the Weber contrast model analysis at different illuminating angles in foggy conditions. Legend: 0°, 5°, 10°, 15°, 20°, 25°, 30°, 35°, 40°, 45°, 50°, 55°, 60°, 65°, 70°, 75°, 80°, 85°.

4.3. Results

First, from the experimental results obtained in Section 3.3., the fog luminance was retrieved for each illuminating angle. Figure 7 shows J_{fog} computed according to (20), by replacing $R_{\text{TOT}} = R_{\text{ST}} + R_{\text{TO}}$ and $\sigma = 3/MOR$, but expressed in camera pixel intensity. As it is possible to observe, the fog luminance depends on the illuminating angle, becoming more intense for small angles. Moreover, as expected, it depends also on the visibility level, since lower visibility means more dense fog and thus higher fog luminance.

Applying J_{fog} to the model, we derived the Weber contrast C_{m} shown by Figure 8. As with the experimental results, the discussion of model results will be discussed in Section 5..

5. DISCUSSION OF THE RESULTS

In this section, the results presented previously are analyzed and discussed and compared.

The experimentally obtained contrast curves shown in Figure 5 exhibit the behavior anticipated in Section 2.2.. Specifically, the Weber contrast for the camera signal, in the case of a target that is less luminous than the background (i.e., a black target on

a white background), assumes negative values and ranges from -1 (high contrast) to 0 (high contrast). The contrast exhibits a hyperbolic decay with decreasing MOR and approaches zero under conditions of dense fog. Under favorable visibility conditions, as expected, the experimental Weber contrast C_{e} is essentially independent of the illumination angle, attaining approximately the same value for $MOR > 40\,\mathrm{m}$. For MOR values between 0 m and 40 m, it is observed that, for intermediate illumination angles (from $\alpha = 30°$ to $\alpha = 65°$), the contrast reaches its saturation level more rapidly than in the extreme angular cases ($\alpha \leq 25°$ and $\alpha \geq 70°$). This behavior can be interpreted by assuming that the fog luminance component has a reduced influence in this angular range.

With regard to the empirical model, it can be observed that the corresponding results exhibit the same qualitative behavior as the experimental data. In particular, the contrast C_{m} replicates the behavior of C_{e} with high fidelity, apart from a slightly different saturation level. This discrepancy is most likely attributable to the fact that the black region of the experimental target is not perfectly black, preventing it from reaching the theoretical maximum contrast ($C_{\mathrm{m}} = -1$). The output of the interpretative model therefore shows how contrast has a hyperbolic relationship with respect to MOR precisely, because of the presence of fog luminance. Indeed, for low MOR values (corresponding to low transmittance values T), the Weber contrast scales as $1/L_{\mathrm{fog}}$, according to equations (23) and (24). Consequently, the larger the fog luminance component, the more slowly C varies, with respect to MOR, in order to reach its saturation value. This result therefore shows that MOR, considering only light attenuation, does not fully represent the visibility perceived by an observer or a vision-based system. On the contrary, contrast provides information that is more consistent with what is actually perceived by an observer.

6. CONCLUSIONS

The aim of this study was to compare the MOR and the visibility that can be evaluated from the analysis of the image contrast by varying the illumination geometry in a foggy environment. As expected, the MOR is not able to accurately describe the phenomena caused by fog-generated scattering. Conversely, Weber contrast, based on luminance, takes into account the presence of back-scattering and veiling, providing more accurate information about the actual visibility in a foggy environment. The experimental results demonstrate that the contrast has a hyperbolic relationship with the MOR, showing a behavior which depends on the illumination angle, which modifies the observed contrast, primarily through variations in fog luminance. The simplified model developed in this work, which is based on measured luminance and an empirical characterization of fog luminance, is able to reproduce the experimental trends and highlights that the difference in the behavior of MOR and contrast is given by the presence of fog luminance L_{fog}. Moreover, the results show the dependence of "perceived" visibility on the specific source–target–sensor configuration.

REFERENCES

[1] M. Ballesta-Garcia, S. P. na Gutiérrez, A. Rodríguez-Aramendía, P. García-Gómez, N. Rodrigo, A. R. Bobi, S. Royo, Analysis of the performance of a polarized lidar imager in fog, Opt. Express, vol. 30, Nov 2022, no. 23, pp. 41 524–41 540.
DOI: 10.1364/OE.471872

[2] M. Dreissig, D. Scheuble, F. Piewak, J. Boedecker, Survey on lidar perception in adverse weather conditions, 2023 IEEE Intelligent Vehicles Symposium (IV), 2023, pp. 1–8.
DOI: 10.1109/IV55152.2023.10186539

[3] M. Kutila, P. Pyykönen, H. Holzhüter, M. Colomb, P. Duthon, Automotive lidar performance verification in fog and rain, 2018 21st International Conference on Intelligent Transportation Systems (ITSC), 2018, pp. 1695–1701.
DOI: 10.1109/ITSC.2018.8569624

[4] F. Sezgin, D. Vriesman, D. Steinhauser, R. Lugner, T. Brandmeier, Safe autonomous driving in adverse weather: Sensor evaluation and performance monitoring, 2023 IEEE Intelligent Vehicles Symposium (IV), 2023, pp. 1–6.
DOI: 10.1109/IV55152.2023.10186596

[5] D. Cassanelli, S. Cattini, G. Di Loro, L. Di Cecilia, L. Ferrari, D. Goldoni, L. Rovati, A simple method for the preliminary analysis and benchmarking of automotive lidars in fog, 2022 IEEE International Instrumentation and Measurement Technology Conference (I2MTC), 2022, pp. 1–6.
DOI: 10.1109/I2MTC48687.2022.9806549

[6] D. Cassanelli, S. Cattini, L. Medici, L. Ferrari, L. Rovati, A simple experimental method to estimate and benchmark automotive lidars performance in fog, Acta IMEKO, vol. 13, 2024, no. 4, pp. 1–8.
DOI: 10.21014/actaimeko.v13i4.1885

[7] Y. Li, P. Duthon, M. Colomb, J. Ibanez-Guzman, What happens for a tof lidar in fog? IEEE Transactions on Intelligent Transportation Systems, vol. 22, 2021, no. 11, pp. 6670–6681.
DOI: 10.1109/TITS.2020.2998077

[8] W. M. O. (WMO), Guide to instruments and methods of observation, (wmo-no. 8), Geneva, Switzerland, vol. 3, 2024.
DOI: 10.59327/WMO/CIMO/3

[9] ISO-28902-1:2012, Air quality–environmental meteorology–part 1: Ground-based remote sensing of visual range by lidar, 2012.

[10] N. Graves, S. Newsam, Camera–based visibility estimation: Incorporating multiple regions and unlabeled observations, Ecological Informatics, vol. 23, 2014, pp. 62–68.
DOI: 10.1016/j.ecoinf.2013.08.005

[11] L. Chen, Z. Yu, H. Wang, S. Wang, X. Liu, L. Mei, J. Zheng, P. Zuo, Error analysis and visibility classification of camera-based visiometer using svm under nonstandard conditions, Atmosphere, vol. 14, 2023, no. 7.
DOI: 10.3390/atmos14071105

[12] N. Hautiére, R. Babari, É. Dumont, R. Brémond, N. Paparoditis, Estimating meteorological visibility using cameras: A probabilistic model-driven approach, Asian Conference on Computer Vision, Springer, 2010, pp. 243–254.
DOI: 10.1007/978-3-642-19282-1_20

[13] S. Yeo, Y. Nalcakan, Y. Jin, I. Park, H. Ju, S. Kim, Seeing through the rain: An empirical assessment of short-wave infrared imaging on enhancing autonomous vehicle perception under rainy weather, Measurement, vol. 259, 2026, p. 119654.
DOI: 10.1016/j.measurement.2025.119654

[14] Z. Li, S. Zhang, Z. Fu, F. Meng, L. Zhang, Confidence-feature fusion: A novel method for fog density estimation in object detection systems, Electronics, vol. 14, 2025, no. 2.
DOI: 10.3390/electronics14020219

[15] E. Peli, Contrast in complex images, Journal of the Optical Society of America A, vol. 7, 1990, no. 10, pp. 2032–2040.
DOI: 10.1364/JOSAA.7.002032

[16] J. Qian, B. Kong, J. Yang, C. Wang, Research on contrast calculation method for color image, Chinese Conference on Image and Graphics Technologies, Springer, 2023, pp. 239–253.
DOI: 10.1007/978-981-99-7549-5_18

[17] G. Paulmier, Fog luminance evaluation in daytime, Transportation research record, vol. 1862, 2004, no. 1, pp. 82–88.
DOI: 10.3141/1862-10

[18] J. Quintana Benito, A. A. Fernández-Balbuena, J. C. Martínez-Antón, D. Váquez Molini, Improvement of driver night vision in foggy environments by structured light projection, Heliyon, vol. 8, 2022, no. 11, p. e11877.
DOI: 10.1016/j.heliyon.2022.e11877

[19] W. R. McCluney, Introduction to radiometry and photometry, Artech House, 2014, ISBN: 978-1-60807-833-2.
[20] W. E. K. Middleton, Vision through the atmosphere, Springer, 1957.
DOI: 10.1007/978-3-642-45881-1_3
[21] V. E. Zuev, Propagation of Visible and Infrared Radiation in the Atmosphere, John Wiley & Sons, 1974.
[22] E. Dumont, N. Hautière, R. Gallen, A semi-analytic model of fog effects on vision, Atmospheric Turbulence, Meteorological Modeling and Aerodynamics, vol. 5, 2010.
[23] H. Gross, F. Blechinger, B. Achtner, Handbook of optical systems, Wiley Online Library, 2005, vol. 1.
DOI: 10.1002/9783527699247